A NUMERICAL METHOD OF ESTIMATING AND OPTIMIZING THE SUPERSONIC AERODYNAMIC CHARACTERISTICS OF WINGS OF ARBITRARY PLANFORM

Wilbur D. Middleton and Harry W. Carlson

NASA Langley Research Center
Langley Station, Hampton, Va.

AIAA Paper
No. 64-590

AIAA TRANSPORT AIRCRAFT DESIGN & OPERATIONS MEETING

SEATTLE, WASHINGTON AUGUST 10-12, 1964

A NUMERICAL METHOD OF ESTIMATING AND OPTIMIZING THE SUPERSONIC AERODYNAMIC CHARACTERISTICS OF WINGS OF ARBITRARY PLANFORM

Wilbur D. Middleton and Harry W. Carlson
Aerospace Engineers, Supersonic Mechanics Section
Full-Scale Research Division
NASA Langley Research Center

Introduction

The continuing and recently accentuated search for aerodynamically efficient supersonic transport designs necessitates not only the fullest use of existing technology, but also requires the development of new analytical methods of evaluating potentially efficient configurations. Because of the large portion of total airplane drag associated with the generation of lift, there is need for a thorough study of design concepts offering the possibility of reduction of this drag component.

The wing planform, which is of primary importance in its effect on drag at lifting conditions, in past studies has been largely restricted to straight line leading and trailing edges. Such limitations have resulted mainly from a lack of analytical methods for estimating the aerodynamic characteristics of wings of arbitrary planform. This deficiency may now be overcome by application of modern digital computers to the solution of linearized theory integral equations for wing planforms which may employ curved or cranked leading and trailing edges. Computer programs such as those discussed in this paper greatly expand the possibilities for the development of truly efficient supersonic airplane configurations.

This paper illustrates the application of numerical methods to wing camber surfaces of arbitrary planform, to obtain the surface shape required to support a specified pressure distribution or, inversely, to obtain the pressure distribution on wings of specified shape. Two special cases are noted and demonstrated: in the direct solution, the surface shape corresponding to an optimum combination of loadings (for least drag at a specified lift) may be obtained; in the inverse solution, the pressure distribution on a flat wing of arbitrary planform may be obtained.

Used in combination, the numerical methods allow the determination of linear theory drag-due-to-lift polars and lift-moment relationships for wings of arbitrary planform which may employ any specified surface shape. With attention given to the real flow considerations that limit the application of linear theory,[1] studies of the aerodynamic characteristics of arbitrary wing planforms with various surface shapes may be analytically conducted.

To illustrate the use of the method, a set of examples is presented for a typical planform series. The agreement obtained between the numerical method and experiment is shown in a second set of examples, employing both flat and warped wing surfaces.

author

Symbols

$A(L,N)$	leading-edge grid element weighting factor
b	wing span
C_D	drag coefficient
$C_{D,min}$	zero-lift drag coefficient of flat-wing configuration
ΔC_D	drag coefficient due to lift, $C_D - C_{D,min}$
C_m	pitching-moment coefficient
$C_{m,o,F}$	zero-lift pitching-moment coefficient of flat-wing configuration
$\Delta C_m = C_m - C_{m,o,F}$	
C_L	lift coefficient
$C_{L,\alpha}$	lift-curve slope per degree angle of attack
C_p	pressure coefficient
ΔC_p	lifting pressure coefficient
l	overall length of wing measured in streamwise direction
L,N	designation of influencing grid elements
L^*,N^*	designation of field-point grid elements
M	Mach number
$\bar{R}$	average value of influence function within a grid element
x,y,z	Cartesian coordinate system, x-axis streamwise
x_{cp}	x-coordinate of wing center of pressure
z_c	camber surface ordinate
$\Delta z_c = z_c - z_{c,le}$	
α	wing angle of attack, deg

$\beta = \sqrt{M^2 - 1}$

ξ, η dummy variables of integration for x and y, respectively

τ designates a region of integration bounded by the wing planform and the fore Mach cone from the point x,y

Λ wing leading-edge sweepback angle

Subscripts:

F, W, WF, FF designates various drag components (see fig. 7)

Discussion

A typical wing planform described by a rectangular Cartesian coordinate system is illustrated in figure 1. Overlaid upon the wing planform is the grid system used in the numerical solution of the linear theory integral equation. A mosaic of whole and partial grid elements approximates the actual wing planform and surface shape. In accordance with the assumptions of linear theory, the wing has negligible thickness, and lies essentially in the $z = 0$ plane.

In the numerical approach, the grid elements, identified by L and N, are arranged such that L is numerically equal to x and N is numerically equal to βy, where x and βy take on only integer values. Partial grid elements along the wing leading and trailing edges are used to permit a closer approximation to the actual wing planform. The grid system of figure 1 is rather coarse for illustrative purposes; in actual usage, many more grid elements are employed.

With respect to a specified field point x,y, the upstream region of influence τ (bounded by the fore Mach cone from x,y and the wing leading edge), is approximated by the shaded grid elements of figure 1. Each of these elements has associated with it an influence factor $\bar{R}$ which relates the effect of the element and its average pressure to the surface slope required to obtain a specified lifting pressure at x,y. The factor $\bar{R}$ is determined from an approximate solution to the linear theory integrals over the region bounded by the individual elements.

The variation of $\bar{R}$ within the fore Mach lines from the field point and the corresponding grid element (L^*,N^*) is illustrated in figure 2. For a set of elements at a constant $L^* - L$ value, the sum of the $\bar{R}$ values is zero, the single negative value at $N^* = N$ balancing all the others. Where $L^* = L$, only a single element is contained within the Mach lines, and $\bar{R} = 0$.

The basic equation relating the required surface slope at x,y to a prescribed pressure distribution, written in the form of the numerical solution, is equation (1) of figure 2.[2] The effect of the upstream elements within τ is included in the summation term, which adds directly to the prescribed lifting pressure coefficient at the field element to define the necessary surface slope. In this equation, the factor A(L,N) accounts for partial grid elements, being equal to the element length in the x-direction.

Equation (2), a rearrangement of equation (1), provides a solution to the inverse problem, that of solving for the lifting pressure coefficient corresponding to a specified surface shape.[3] In this equation the summation term utilizes previously determined lifting pressure coefficients, which are computed following a prescribed order of calculation, i.e., from apex aft. With this procedure, and utilizing the fact that $\bar{R}(N^*,L^*)$ is zero, no unknown pressure coefficients arise in the numerical summations.

The wing surface slope variation required in equation (2) is provided by supplemental calculations, which consist of determining the streamwise inclination of all grid elements from a set of camber surface ordinates. The flat wing at a small angle of attack represents a special case of equation (2), in which $\frac{\partial z}{\partial x}(L^*,N^*)$ is a constant.

The precision of the numerical method in defining the theoretical surface shape required to support a specified pressure distribution on wings of arbitrary planform has been illustrated in an NASA report.[2] Similar illustrations involving the inverse solution are contained in an NASA prospective report,[3] from which a typical example is included here to show the type of detailed pressure distributions obtained from the numerical method, and the departures from more rigorous solutions. In figure 3 numerical solution pressure distributions for a flat double-delta planform at two Mach numbers are compared with results from a superposition analysis.[4] Agreement between the two pressure distributions is generally quite good, although the numerical solution does not produce the sharp pressure peaks along Mach lines that characterize the superposition analysis. Comparisons of total wing lift coefficient and center of pressure between the two solutions show reasonably good agreement as follows:

	M = 1.414		M = 1.667	
	$C_{L,\alpha}$	x_{cp}/l	$C_{L,\alpha}$	x_{cp}/l
Superposition analysis	0.0514	0.682	0.0461	Not given
Numerical solution	.0507	.687	.0449	.686

The use of the numerical methods to obtain camber surfaces for wings having a prescribed loading, and pressure distributions for flat wings of the same planform is illustrated in figures 4 and 5 for a series of wings having the same span and length. The three wings have delta, ogee, and blunt ogive planforms, oriented with respect to the apex Mach lines such that the sweepback parameter (β cot Λ) of the delta wing is 0.70.

In figure 4, the surface shape and loading distributions are shown for an optimum combination (having least drag at a specified lift coefficient)

of a uniform, linear spanwise, and linear chordwise loading, calculated by the numerical method. The corresponding drag-due-to-lift factors are also tabulated. The general characteristics of the required surface shape for the delta and ogee planforms are quite similar, both exhibiting the extreme root incidence predicted by linear theory for wings with a sharp apex. The ogee wing has more abrupt surface curvature near the wing root, however, and remains nearly flat over the outboard 60-percent span. In contrast, the blunt ogive planform exhibits much more moderate surface slopes, and less variation in surface pressures. The drag-due-to-lift factor of the ogee planform is the lowest of the three. The highest drag factor is obtained with the blunt ogive planform, 20 percent higher than the ogee; however, since only moderate camber is required, that value may be more easily attained in practice.

The corresponding set of pressure distributions for flat wings of the same planform series is presented in figure 5. In this figure, the surface of the flat plate is shown in the same coordinate system as used in the previous figure to facilitate comparisons. All of the pressure distributions exhibit the extreme leading-edge pressures associated with linear theory analyses of subsonic leading-edge wings. In the supersonic leading-edge portion of the blunt ogive wing, and the areas near the locally supersonic leading edge of the ogee planform, a general reduction of the pressure-distribution peaks may be observed. The drag-due-to-lift factors of the flat-plate solution represent only the drag component caused by the rearward inclination of the normal-force vector at angles of attack, and do not include any of the theoretical "leading-edge-suction" force.

The two solutions of figures 4 and 5 may be combined to produce a conventional force coefficient presentation, of drag-due-to-lift and pitching moment versus lift, if a design lift coefficient is selected so that a particular camber surface may be defined. This is done in figure 6 for three wings of the series. In this comparison, the wing shape in each case is that required by the optimum combination of loadings for minimum drag at a design lift coefficient of 0.10. The variation in drag coefficient and pitching-moment coefficient with increments in lift coefficient away from 0.10 is defined by the flat-wing characteristics, using a subsequently discussed superposition technique. The lowest drag-due-to-lift factor, highest degree of static stability, and largest value of zero-lift moment are obtained with the ogee planform. (For this comparison, all moment coefficients were based on the wing length and taken about the 50-percent length.) However, the camber surface for the ogee planform also requires the most severe departures from the $z = 0$ plane, with corresponding departures from linear theory assumptions.

The selection of the planform series of figures 4, 5, and 6 was arbitrary; the use of other selection criteria would likely result in different conclusions regarding the planforms. The illustration intended is that the numerical methods offer a useful tool in studying tradeoffs between various planform geometries established by a set of basic ground rules.

The use of the numerical solutions is not restricted to the design application, where an optimum or other specified loading is desired. The general case of the inverse solution may also be handled, that of obtaining the pressure distributions on a specified warped wing surface throughout a lift-coefficient range. Such a capability is of great utility, both with respect to obtaining the theoretical aerodynamic characteristics of a design surface at off-design Mach numbers, and with respect to estimating the effect of modifying a theoretical surface geometry because of imposed physical constraints.

The construction of a drag polar for a warped surface utilizes a superposition technique, involving the calculation of the drag and lift coefficients of the surface at a selected angle of attack; the calculation of the drag and lift coefficients of the corresponding flat-wing planform per unit angle of attack; the interference drag of the flat-wing pressures acting on the warped surface; and the interference drag of the warped-wing pressures acting on the flat-wing surface, all of which are readily handled by the numerical approach. The technique of combining these force coefficients into a composite drag polar for the warped surface is illustrated in figure 7. This composite polar considers drag-due-to-lift only; however, with the addition of appropriate drag increments for thickness effects and skin friction, a complete polar can be constructed for a wing or wing body.

The construction of the $C_m - C_L$ curve for the warped wing is more direct, consisting of shifting the flat-wing $C_m - C_L$ curve to pass through the moment coefficient of the warped wing at its corresponding lift coefficient.

A comparison between numerical solution force coefficients and corresponding experimental data is presented in figure 8 for a wing-body with an uncambered ogee wing. Experimental data for this configuration was obtained at three Mach numbers;[8] the numerical method data were calculated for the complete wing-body planform shown in the inset sketch. Agreement between the experimental and numerical method data is quite good, both in the moment and drag-due-to-lift comparisons.

Similar comparisons between the numerical solution and experiment for both flat and warped wings, at and off-design Mach numbers, are presented in figures 9 and 10 for arrow and ogee planforms. The warped wings of these figures were basically designed according to a restricted twist and camber approach,[1,5] which limits the allowable degree of surface warpage in view of real flow considerations. However, even with these restrictions, a singularity[2] occurs in the camber surface near the wing root which must be adjusted empirically to provide a reasonable root incidence angle. In calculating the theoretical aerodynamic characteristics of these warped wings the actual camber surface shape that was tested was used.

The force coefficient comparison for the arrow wings is shown in figure 9. The wings are the flat and 0.08 design-lift-coefficient versions of a 70° sweepback family.[5,6] Data are presented for the design Mach number 2.0 and off-design Mach numbers of 1.6 and 2.2. (In this and subsequent figures, the ΔC_D of the experimental data is with respect to the minimum drag coefficient of the flat-wing configuration, and the ΔC_m is with

respect to the zero-lift pitching-moment coefficient of the flat-wing configuration.) The numerical method predicts reasonably well the experimental drag-due-to-lift variation of the two wings with Mach number, particularly with respect to the reduction of the drag-due-to-lift difference between the flat and warped wings with increasing Mach number. Reasonably good agreement between experiment and the numerical solution is also obtained in the zero-lift moment increment ΔC_{m_o} between the two wings; however, nonlinearities in the experimental pitching-moment data make agreement poor at lift coefficients above approximately 0.10. It may be observed that the flat-wing drag measurements at lift coefficients on the order of 0.10 are lower than the theoretical estimate (Mach numbers 1.6 and 2.0). This behavior is believed caused by a leading-edge vortex,[7] not included in the linear theory analysis.

Also in figure 9, the drag-due-to-lift envelope polar of the three-component optimum loading is shown at Mach number 2.0 for the arrow wing planform. The increment in drag coefficient between the optimum envelope and the warped-wing polar at the design lift coefficient of 0.08 is a measure of the theoretical drag penalty of the restricted twist and camber wing, as opposed to a theoretically optimized shape. However, since experimental attempts to verify the applicability of the unrestricted optimum concept of linear theory have been largely unsuccessful,[1] this theoretical drag penalty is rather meaningless. Considerably more success has been obtained in experimentally verifying limited forms of the optimum theory; the restricted twist and camber approach[1] is one reasonably successful technique of limiting the local surface slopes of a wing camber surface so that linear theory can be used to predict the aerodynamic characteristics of the wing.

The ogee planform comparison is presented in figure 10 with force coefficients from the numerical method and unpublished experimental data shown for a wing-body configuration. (The wing planform for the numerical solution was again taken as the complete projected wing-body shape.) Both flat and warped wings were tested, the warped version being designed initially for $C_L = 0.10$ at a Mach number of 2.2, using the numerical method[2] and the restricted twist and camber approach. However, empirical modifications to the warped wing were incorporated in the course of the testing, so that it was necessary to scale the wing shape of the final test configuration from the model for the inverse method calculations. The numerical method drag polar is seen to agree reasonably well with the experimental data, particularly at the higher Mach numbers; an apparent vortex effect is evident in the drag data of both wings at Mach number 1.8. In the pitching-moment comparison, the numerical method is seen to predict quite well the increment in moment between the flat and warped wings, and to estimate the stability levels reasonably well. However, nonlinear pitching-moment effects may be observed in the experimental data at the higher lift coefficients, particularly in the case of the warped wing.

Concluding Remarks

While any technique employing linearized theory must be employed judiciously in order for the solution to be applicable in the real flow case, reasonable agreement obtained between data from experiment and the numerical methods for various wing configurations has verified the general usefulness of the numerical techniques. The use of the numerical methods to extend the application of linear theory analyses to wings having a wide variety of planform and surface shapes offers significantly expanded possibilities for the development of aerodynamically optimized supersonic aircraft.

References

1. McLean, F. Edward, and Fuller, Dennis E.: Supersonic Aerodynamic Characteristics of Some Simplified and Complex Aircraft Configurations Which Employ Highly Swept Twisted-and-Cambered Arrow-Wing Planforms. Vehicle Design and Propulsion. American Inst. Aero. and Astronautics, November 1963, pp. 98-103.

2. Carlson, Harry W., and Middleton, Wilbur D.: A Numerical Method for the Design of Camber Surfaces of Supersonic Wings With Arbitrary Planforms. NASA TN D-2341, 1964.

3. Middleton, Wilbur D., and Carlson, Harry W.: A Numerical Method for Calculating the Flat Plate Pressure Distributions on Supersonic Wings of Arbitrary Planform. NASA Prospective TN.

4. Cohen, Doris, and Friedman, M. D.: Theoretical Investigation of the Supersonic Lift and Drag of Thin, Sweptback Wings With Increased Sweep Near the Root. NACA TN 2959, 1953.

5. Carlson, Harry W.: Aerodynamic Characteristics at Mach Number 2.05 of a Series of Highly Swept Arrow Wings Employing Various Degrees of Twist and Camber. NASA TM X-332, 1960.

6. Middleton, Wilbur D., and Sorrells, Russell B.: Off-Design Aerodynamic Characteristics at Mach Numbers 1.61 and 2.20 of a Series of Highly Swept Arrow Wings Designed for Mach Number 2.0 Employing Various Degrees of Twist and Camber. NASA TN D-1630, 1963.

7. Carlson, Harry W.: Pressure Distributions at Mach Number 2.05 on a Series of Highly Swept Arrow Wings Employing Various Degrees of Twist and Camber. NASA TN D-1264, 1962.

8. Hicks, Raymond M., and Hopkins, Edward J.: Effects of Spanwise Variation of Leading-Edge Sweep on the Lift, Drag, and Pitching Moment of a Wing-Body Combination at Mach Numbers from 0.7 to 2.94. NASA TN D-2236, 1964.

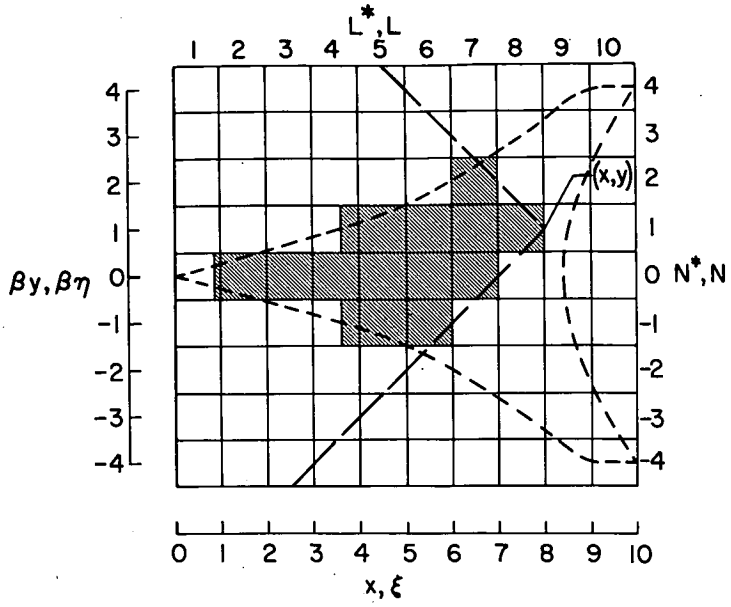

NASA

Figure 1.- Wing coordinate system.

INFLUENCE FACTOR

$\bar{R}\,(L^*-L, N^*-N)$

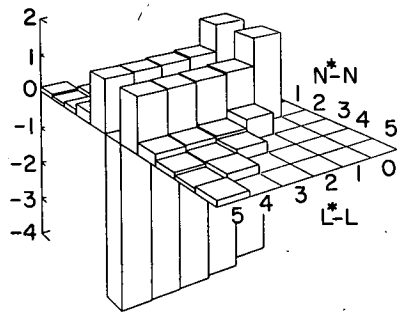

SUMMATIONS

GIVEN LOAD DISTRIBUTION

$$\frac{\partial z_c}{\partial x} = \frac{-\beta}{4}\,\Delta C_p(L^*,N^*) + \frac{\beta}{4\pi}\sum \Delta C_p(L,N)\,A(L,N)\,\bar{R}(L^*-L,N^*-N) \quad (1)$$

GIVEN SURFACE SHAPE

$$\Delta C_p = \frac{-4}{\beta}\,\frac{\partial z_c}{\partial x}(L^*,N^*) + \frac{1}{\pi}\sum \Delta C_p(L,N)\,A(L,N)\,\bar{R}(L^*-L,N^*-N) \quad (2)$$

NASA

Figure 2.- Numerical solution of linearized theory.

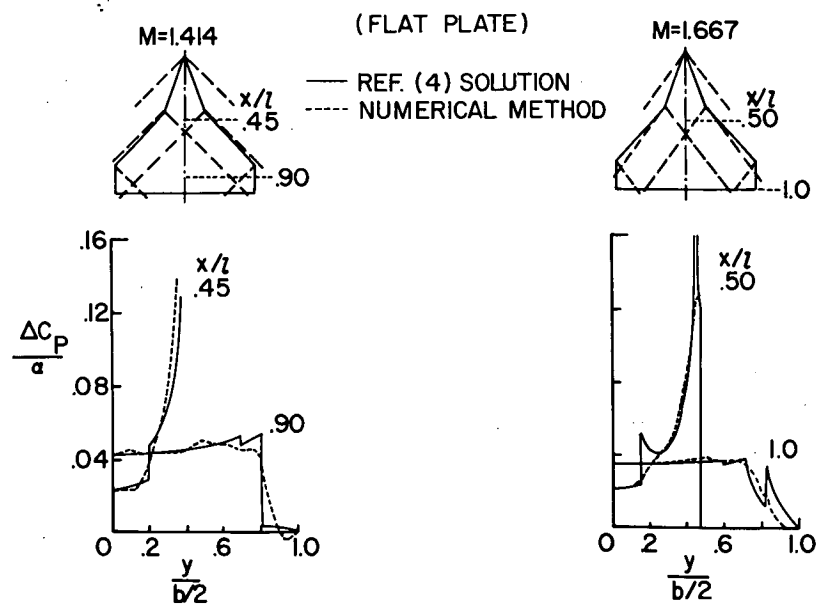

NASA

Figure 3.- Comparison of numerical method with superposition solution.

OPTIMUM COMBINATION

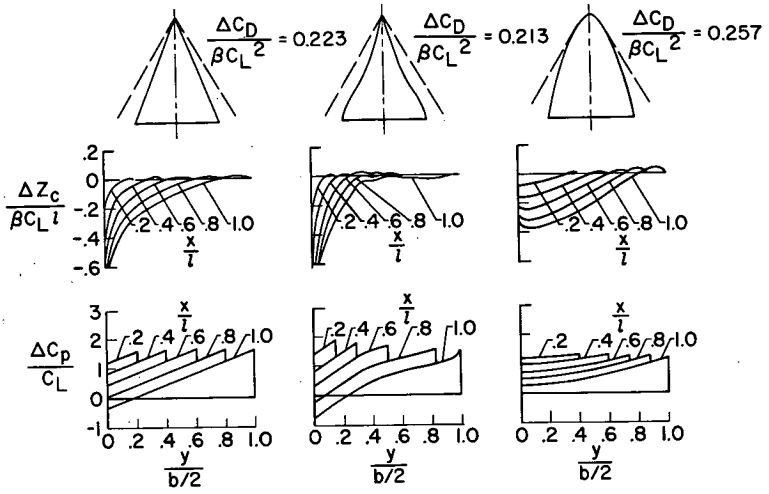

NASA

Figure 4.- Camber surface for a specified loading.

FLAT PLATE

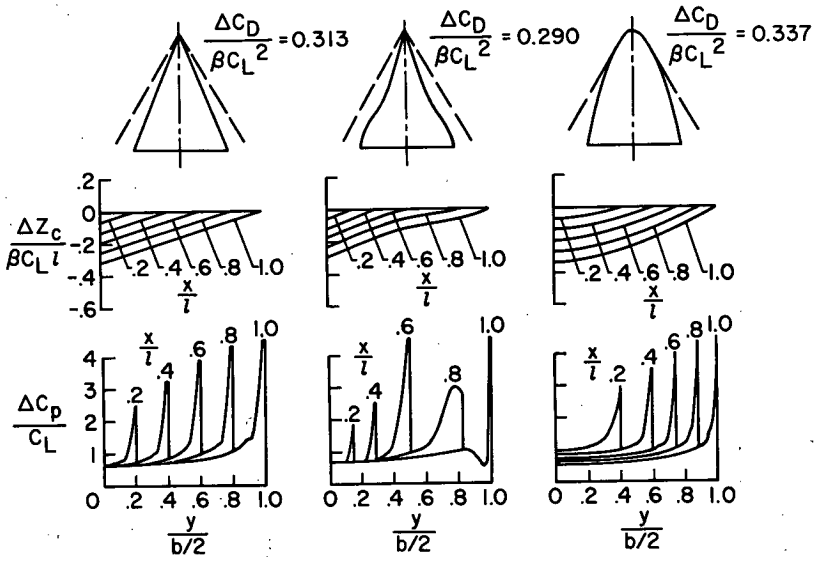

NASA

Figure 5.- Loading for a specified camber surface.

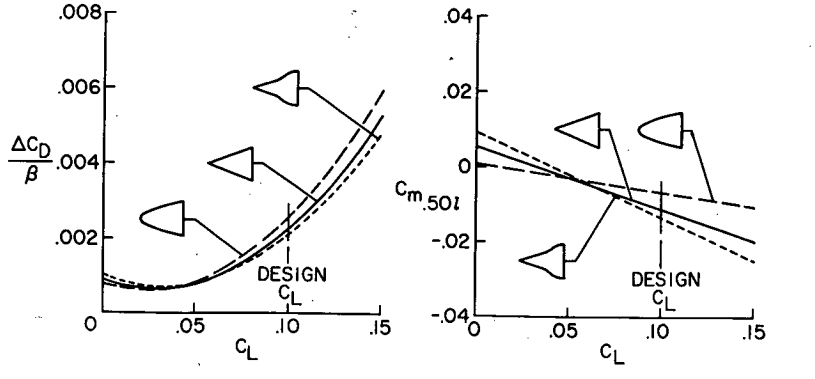

NASA

Figure 6.- Drag and moment characteristics of wing series.

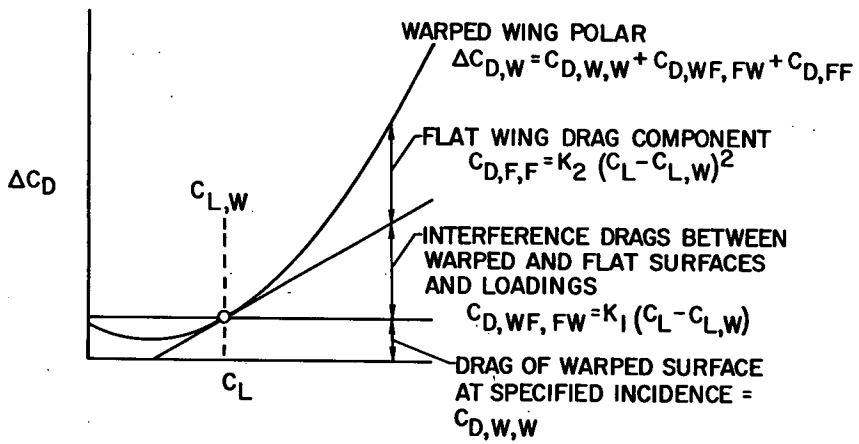

NASA

Figure 7.- Composite drag polar of warped surface.

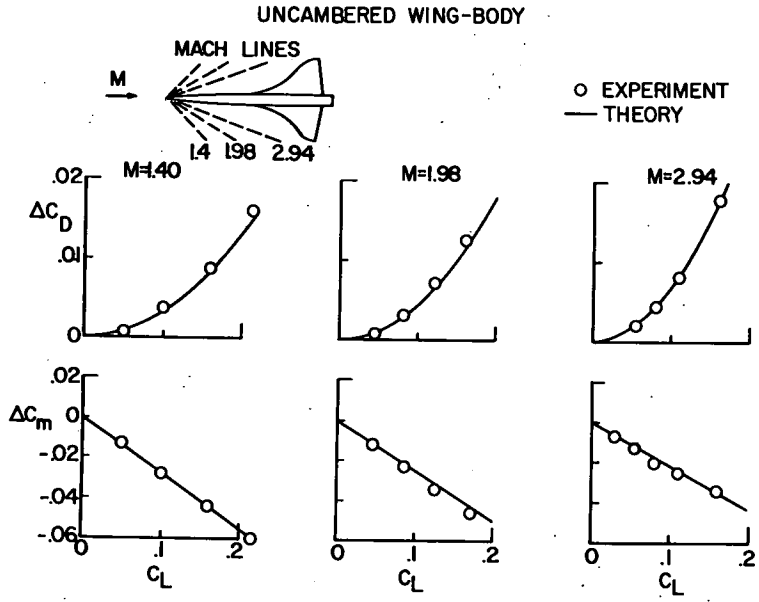

NASA

Figure 8.- Comparison of numerical method with experiment.

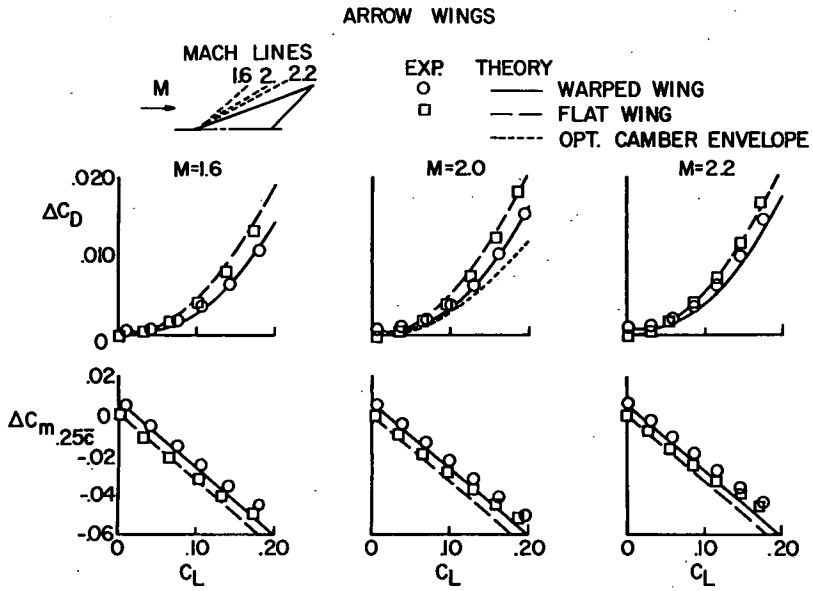

NASA

Figure 9.- Comparison of numerical method with experiment.

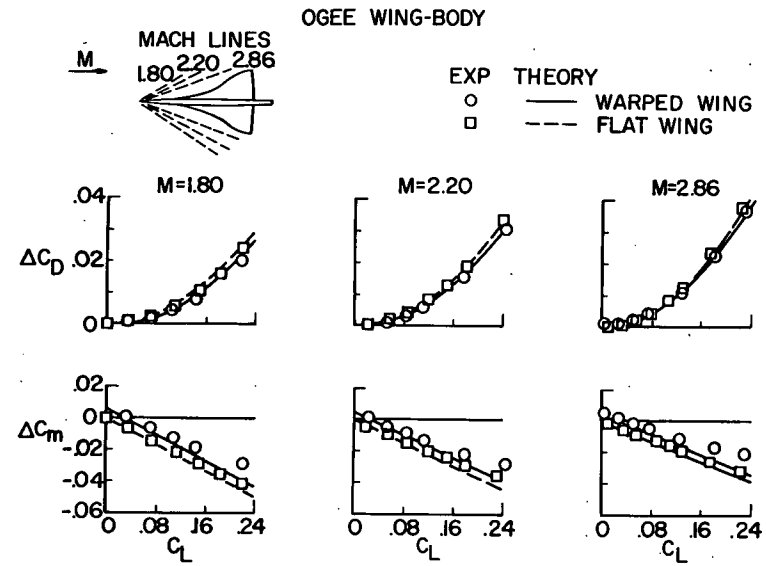

NASA

Figure 10.- Comparison of numerical method with experiment.